

Contents lists available at ScienceDirect

Physica D

journal homepage: www.elsevier.com/locate/physd



Dissolution of plane surfaces by sources in potential flow

Yunshan Jiang, N.R. McDonald*

Department of Mathematics, University College London, London, WC1E 6BT, UK



ARTICLE INFO

Article history:
Received 27 June 2022
Received in revised form 23 August 2022
Accepted 23 September 2022
Available online 4 October 2022
Communicated by B. Protas

Keywords: Conformal mapping Dissolution Interfaces Free boundary

ABSTRACT

The two-dimensional free boundary problem for a surface dissolving in potential flow owing to concentrated sources of dissolving agent c is formulated and solved. The surface boundary evolves quasi-steadily, and the resulting steady advection–diffusion equation for c, and Laplace's equation for the velocity potential form a coupled pair of conformally invariant PDEs. The dynamics of the coupled fluid flow and evolving surface depends on the Péclet number: P = UL/D, where U and L are typical velocity and lengthscales respectively, and D is the diffusivity of c. The conformally invariant property is exploited in finding an equation of the Polubarinova–Galin class for the conformal map from the unit ζ -disk to the evolving domain in physical space. The equation is solved numerically and the time-evolution of the dissolving surface determined. For a single concentrated source with flow initially parallel to a flat surface, a Pe-dependent scallop-like surface shape typically develops. The problem involving a periodic array of concentrated sources aligned parallel to an initially flat surface is also solved.

© 2022 The Author(s). Published by Elsevier B.V. This is an open access article under the CC BY license (http://creativecommons.org/licenses/by/4.0/).

1. Introduction

The interaction between fluid flow and surfaces which evolve in response to erosion, chemical dissolution or freezing/melting effects is, in general, a challenging nonlinear free boundary problem: the flow field depends on the surface shape which, in turn, depends on the local fluid transport properties near the fluid-solid boundary. There is much interest in these processes (e.g. [1]), especially in a geological context where the interaction leads to striking features and patterns spanning lengthscales from centimetres to tens of kilometres. Some specific examples include ramified stream networks [2], ice-stars [3], karst pinnacles [4], yardangs and ventifacts [5], terraces [6,7], and the surface scalloping of caves, beneath ice floes and the Martian landscape e.g. [7-10]. The flowing fluid in these examples can be either ocean, surface- or ground-water, or wind, and the shaping of the landscape can be through abrasion, erosion, sediment transport, precipitation or dissolution.

One class of problems considers the mechanical effect of erosion by the flow of fluid, explicitly linking the normal velocity of the eroding interface with the local fluid shear stress e.g. [11,12]. Another class of problems to which the present work belongs, is based on inviscid flow transporting an agent or species c to which the fluid–solid interface responds by, say, freezing, melting or dissolution. In this work the solid loses mass owing to concentrated sources (see Section 3) of dissolving agent is examined. Equally,

* Corresponding author.

E-mail address: n.r.mcdonald@ucl.ac.uk (N.R. McDonald).

the problem applies to the melting of surfaces in the presence of localised heat sources.

Mathematically, progress can be made by assuming two-dimensional dynamics and, further, that the surface evolves quasi-steadily. The latter assumption is valid when the normal velocity of the surface is much smaller than a typical velocity of the fluid flow, and is normally a good assumption for slowly evolving geological features. Assuming the fluid is inviscid and the flow irrotational, the fluid-surface interaction is governed by a pair of coupled PDEs: Laplace's equation for the velocity potential, and the steady advection-diffusion equation for the species concentration (or temperature) c. After a standard nondimensionalisation the parameter governing the behaviour of the solution of the PDEs is the Péclet number: Pe = UL/D, where Uand L are typical velocity and lengthscales respectively, and D is the diffusivity of c. Remarkably, this pair of PDEs is conformally invariant [13], enabling powerful methods of complex analysis to be employed to find exact and asymptotic (in the limit of small and large Pe number) solutions for the case when the surface boundary remains fixed (e.g. [13,14]), or analytical or numerical solutions for the case when the surface boundary evolves e.g. [15– 17]. In these latter studies, the source of c is at infinity and is advected to the surface by the flow. In contrast, the present work considers the case when c is concentrated at a given point(s) at finite distance from the surface.

The coupling at the fluid-solid interface is provided by a Stefan-type boundary condition which directly links the normal velocity of the surface to the normal gradient of *c* at the boundary. By conformal mapping the physical plane to the interior of

the unit ζ -disk, it is shown in Section 4 the problem reduces to finding the conformal map which satisfies a Polubarinova–Galin-type equation as is common in other two-dimensional free boundary problems e.g. Hele-Shaw problems [18–20], or problems, as here, involving advection and diffusion of c e.g. [15–17, 21,22]. Section 6 describes the numerical approach to solving the Polubarinova–Galin equation and presents results for the evolution of the boundary for uniform flow past an isolated source. Results are extended in Section 7 to consider a periodic array of point sources of c.

2. Problem formulation

Irrotational flow of an inviscid, incompressible fluid in the two dimensional (x, y)-plane is considered. The velocity field is given by $\mathbf{u} = \nabla \phi$, where ϕ is the velocity potential which satisfies the Laplace equation

$$\nabla^2 \phi = 0. \tag{1}$$

Let c(x, y) measure the concentration of some species, or fluid property such as temperature, either of which causes a boundary to dissolve or melt. It is assumed that the flow velocity \mathbf{u} is larger than the normal velocity v_n of the dissolving boundary, so the fluid–surface interaction is quasi-steady. The agent c thus satisfies the steady, advection–diffusion equation with non-dimensional form

$$Pe \mathbf{u} \cdot \nabla c = \nabla^2 c, \tag{2}$$

where Pe = UL/D is the Péclet number computed from the fluid velocity scale U, characteristic length scale L and diffusivity D of c(x, y).

The coupled PDEs (1) and (2) are conformally invariant [13], and this property is exploited in this work and the complex variable z = x + iy used.

On the solid surface the following boundary conditions apply

$$c = 0$$

 $\mathbf{u} \cdot \mathbf{n} = 0$,

$$\frac{d\mathbf{x}}{dt} \cdot \mathbf{n} = -\nabla c \cdot \mathbf{n}. \tag{3}$$

The first of these fixes the concentration of c(x, y) to be zero, the second requires the normal velocity of the fluid flow vanish and the third is the Stefan condition which states that the normal velocity of the solid surface boundary is given by the normal derivative of c(x, y)–see e.g. [15,17]. Here 'outward' means in the direction from the solid surface pointing towards the interior of the fluid domain.

3. Flow past a concentrated source

Consider first uniform flow in the real direction when no surfaces are present. The advection-diffusion equation becomes

Pe
$$\frac{\partial c}{\partial x} = \nabla^2 c + \delta(x, y),$$
 (4)

where a concentrated source of c(x, y) fixed at z = 0 is represented by a delta function forcing term. The solution of (4) is (e.g. [14])

$$c(x,y) = \frac{1}{2\pi} e^{xPe/2} K_0 \left[\frac{Pe}{2} \sqrt{x^2 + y^2} \right], \tag{5}$$

where $K_0()$ is a modified Bessel function.

The next step is to incorporate an infinitely long, straight and fixed wall aligned with the real z-axis along which c(x, 0) = 0.

For uniform flow parallel to the wall with delta function forcing at z = i, the solution for c(x, y) is

$$c(x,y) = \frac{1}{2\pi} e^{xPe/2} \left(K_0 \left\lceil \frac{Pe}{2} |z - i| \right\rceil - K_0 \left\lceil \frac{Pe}{2} |z + i| \right\rceil \right). \tag{6}$$

A plot of the c(x,y) with Pe = 1 is given in Fig. 1(a). The concentration field is skewed downstream owing to advection by the flow parallel to the wall towards increasing x. The result is that the normal derivative of the concentration field (6) $\partial c/\partial y$ evaluated at y=0 is asymmetric as shown in Fig. 1(b). Since the Stefan condition (3) equates the normal derivative of c to the normal velocity of the boundary, the wall will dissolve asymmetrically about x=0. In turn, the flow field will evolve according the changing surface shape. This interaction is a nonlinear free boundary problem and is tackled in the next section using a numerical method based on conformal mapping.

4. The Polubarinova-Galin equation

Using conformal mapping, the free boundary problem in the z-plane is converted to a problem in the interior of unit disk in an auxiliary ζ -plane. Let $z=f(\zeta,t)$ be a time-dependent map from the interior of the unit ζ -disk to the physical domain in the z-plane. The boundary $|\zeta|=1$ maps to the evolving free boundary in the z-plane and $\zeta=0$ maps to the location z=i of the source of c(x,y).

The Stefan boundary condition (3) can be written in complex form as

$$\operatorname{Re}\left[\bar{n}_{z}\frac{dz}{dt}\right] = -\operatorname{Re}\left[\bar{n}_{z}\nabla c\right]$$

$$= -2\operatorname{Re}\left[\bar{n}_{z}\frac{\partial c}{\partial \bar{z}}\right],$$
(7)

where n_z is the complex form of the normal to the surface in the z-plane, and the relation $\nabla \equiv 2\partial/\partial \bar{z}$ has been used.

The form of (7) in the ζ -plane is now derived: the complex form of the normal vector in the z and ζ -plane are related by $n_z = f'n_\zeta/|f'|$ and $\partial c/\partial \bar{z} = (\partial c/\partial \bar{\zeta})/\bar{f'}$, since $z = f(\zeta)$ is a conformal map and its analyticity implies $\partial f/\partial \bar{\zeta} = 0$.

Letting $\zeta = r \exp(i\theta)$ in the ζ -plane, the normal derivative of $c(r, \theta)$ at the boundary $|\zeta| = r = 1$ is

$$2\operatorname{Re}\left[\bar{n}_{\zeta}\frac{\partial c}{\partial \bar{\zeta}}\right] = -\frac{\partial c}{\partial r}\bigg|_{r=1} \equiv \sigma(\theta). \tag{8}$$

Substituting (8) in (7) and the fact that $n_\zeta=\zeta$ on the unit ζ -circle, gives the Polubarinova–Galin equation

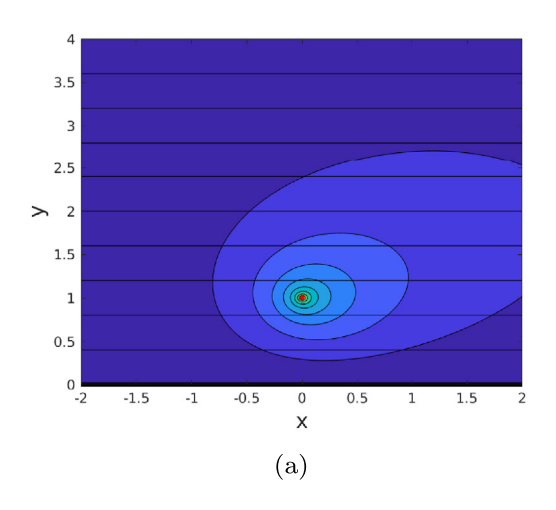
$$\operatorname{Re}\left[\overline{\zeta f'}\frac{\partial f}{\partial t}\right] = \sigma(\theta) \quad \text{on} \quad |\zeta| = 1. \tag{9}$$

The Polubarinova–Galin Eq. (9) expresses the original free boundary problem in the z-plane as a nonlinear equation for the unknown conformal map $f(\zeta,t)$ on the fixed boundary r=1. In order to proceed it is required to find $\sigma(\theta)$. This is done in Section 5.

5. Conformal mapping for the wall dissolution problem

The upper half of the ω -plane has (fixed) fluid-solid interface coinciding with the real ω -axis-see Fig. 2. A point source of c is located at $\omega=i$; c=0 on the real axis and the fluid flow is uniform in the real direction. Thus from (6) the concentration $c(\omega,\bar{\omega})$ and complex potential $F(\omega)$ are

$$c(\omega, \bar{\omega}) = \frac{1}{2\pi} e^{\operatorname{Re}(\omega)\operatorname{Pe}/2} \left(K_0 \left\lceil \frac{\operatorname{Pe}}{2} |\omega - i| \right\rceil - K_0 \left\lceil \frac{\operatorname{Pe}}{2} |\omega + i| \right\rceil \right),$$



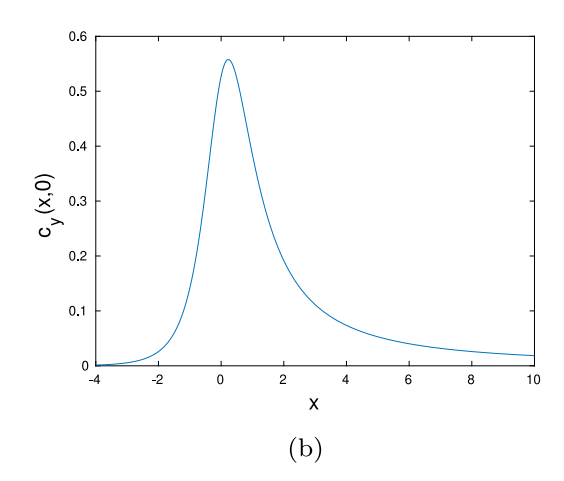


Fig. 1. (a) Concentration field c given by (6) for a source at z = i, Pe = 1 and c = 0 on the real axis, in colour and with equally spaced concentration contours. The streamlines are the lines parallel to the real axis. (b) The normal gradient of c, $\partial c/\partial y$, along the real axis.

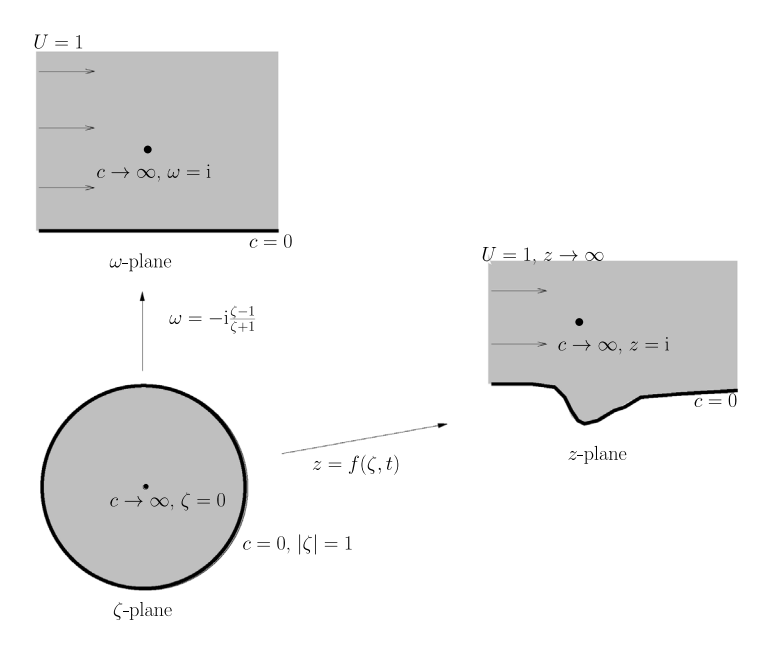


Fig. 2. Conformal maps between the z-, ω - and ζ -planes. The shaded regions map to each other, and c=0 along the boundary (dark lines). The point at which the concentration c is singular is indicated by a small black dot.

$$F(\omega) = \omega. \tag{10}$$

The map

$$\omega = -i\frac{\zeta - 1}{\zeta + 1},\tag{11}$$

maps the interior of the unit ζ -disk to the upper half of the ω -plane with $\zeta=0$ mapping to $\omega=i$, the location of the point source of c. The solution for the species concentration field in the ζ -plane is then

$$c(\zeta, \bar{\zeta}) = \frac{1}{2\pi} \exp\left(\frac{Pe}{2} Re \left[-i\frac{\zeta - 1}{\zeta + 1}\right]\right) \times \left(K_0 \left[Pe \left|\frac{\zeta}{\zeta + 1}\right|\right] - K_0 \left[Pe \left|\frac{1}{\zeta + 1}\right|\right]\right). \tag{12}$$

To find the normal derivative to the boundary $|\zeta| = 1$ in the ζ -plane let $\zeta = r \exp(i\theta)$ so that (12) becomes

$$c(r, \theta) = \frac{1}{2\pi} \exp\left(\frac{\text{Pe} \sin \theta}{r^2 + 1 + 2r \cos \theta}\right) \times$$

$$\left(K_0 \left\lceil \frac{\operatorname{Pe} r}{\sqrt{r^2 + 1 + 2r \cos \theta}} \right\rceil - K_0 \left\lceil \frac{\operatorname{Pe}}{\sqrt{r^2 + 1 + 2r \cos \theta}} \right\rceil \right).$$
(13)

Differentiating (13) with respect to r gives, after simplification, the normal derivative at r=1

$$\frac{\partial c}{\partial r}(1,\theta) = -\frac{1}{2\pi} \exp\left(\frac{\text{Pe}\sin\theta}{2 + 2\cos\theta}\right) K_1 \left[\frac{\text{Pe}}{\sqrt{2 + 2\cos\theta}}\right] \times \frac{\text{Pe}}{\sqrt{2 + 2\cos\theta}}.$$
(14)

In general the conformal map $z=f(\zeta)$ from the ζ -plane to the (physical) z-plane can be written as the series

$$f(\zeta) = \frac{\mathrm{i}A(t)}{\zeta + 1} + \sum_{n=0}^{\infty} \mathrm{i}(a_n(t) + \mathrm{i}b_n(t))\zeta^n, \tag{15}$$

where A(t), $a_n(t)$ and $b_n(t)$ are real coefficients. The point $\zeta=-1$ maps to $z=\infty$. At t=0 the ω - and z-planes coincide, thus A(0)=2, $a_0(0)=-1$ and all other $a_n(0)$ and $b_n(0)$ are zero. Requiring that the source maps to z=i implies f(0)=i and so $A+a_0=1$ and $b_0\equiv 0$.

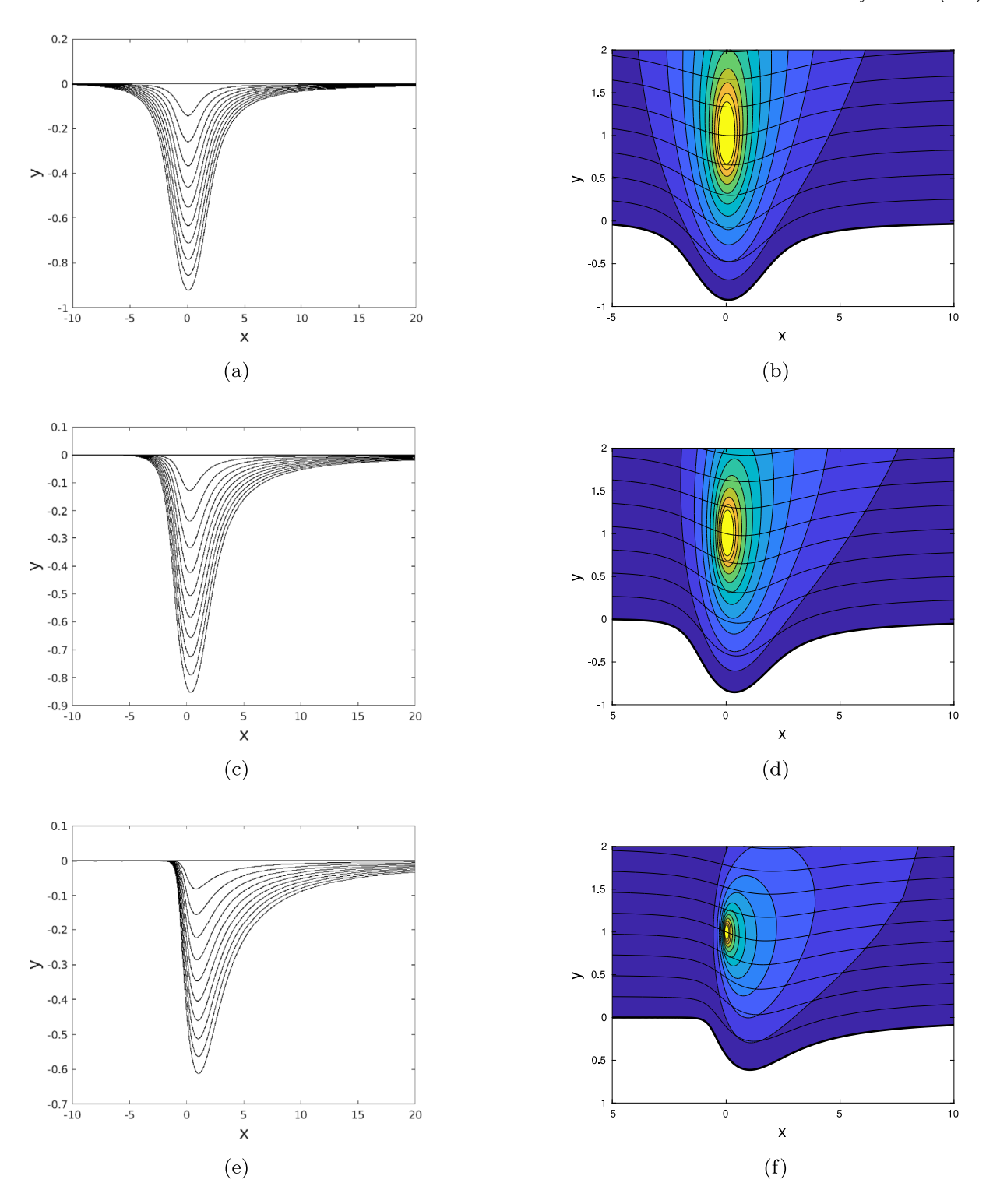


Fig. 3. The left hand plots show the evolving interface at uniform time intervals up to t = 5, and the right hand plots show the concentration field and streamlines at the final time. Three different Pe are shown: (a) and (b) Pe = 1/4; (c) and (d) Pe = 1; (e) and (f) Pe = 4.

Taking the conjugate of (15) and using $\bar{\zeta}=\zeta^{-1}$ on the interface gives the following relation satisfied on the boundary

$$\overline{f(\zeta)} = f(\zeta) - iA - i\sum_{n=0}^{\infty} (a_n + ib_n)(\zeta^n + \zeta^{-n}).$$
(16)

Demanding that the interface in the *z*-plane tends to the real axis far from the source implies that $\bar{f}=f$ in the limit $\zeta\to-1$ and

S

$$A + 2\sum_{n=0}^{\infty} (-1)^n a_n = 0.$$
 (17)

Fig. 2 gives the relation between maps (11) and (15) and the z, ω - and ζ -planes. In summary, the mathematical problem is to

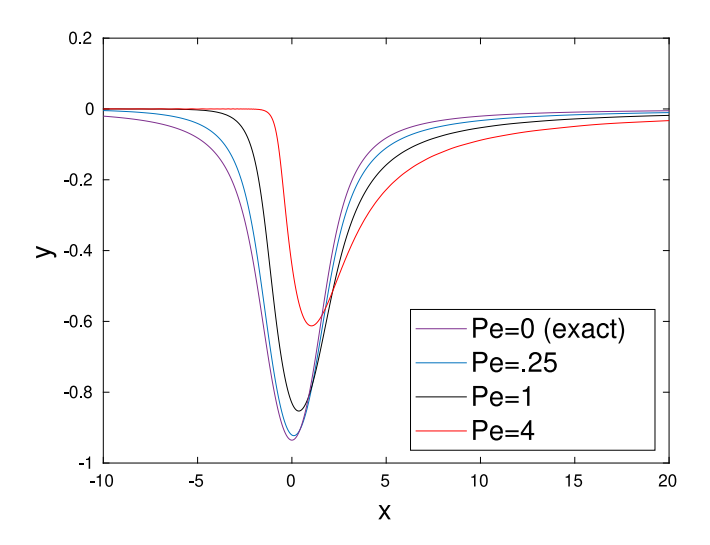


Fig. 4. Comparison of the computed interface profiles at t=5 for different Pe, along with the exact solution for Pe = 0 obtained from (19) and (20).

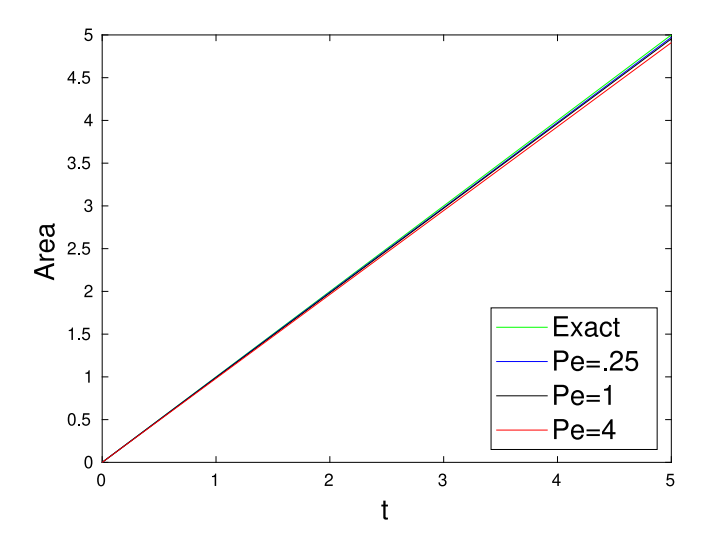


Fig. 5. The dissolved area S as a function of time for the numerical experiments with three different Pe shown in 3, and the exact solution S = t.

solve the Polubarinova–Galin Eq. (9) for the unknown map (15)

$$\operatorname{Re}\left[\overline{\zeta f'(\zeta)}\frac{\partial f}{\partial t}\right] = \sigma(\theta),\tag{18}$$

where $\sigma(\theta) = -\partial c/\partial r$ on r=1 is given by (14). The solution to (18) takes the form (15) subject to conditions (17) and $A+a_0=1$, and initial conditions A(0)=2, $a_0(0)=-1$, $a_n(0)=b_n(0)=0$, n>1.

5.1. Exact solution for Pe = 0

In the limit Pe \to 0 it follows from (14) that $\sigma(\theta) \to 1/2\pi$. In this case (18) has the exact solution (see Appendix A for its derivation)

$$f(\zeta) = \frac{2i}{1+2a} \left(\frac{1}{\zeta+1} + a\zeta + a - \frac{1}{2} \right),\tag{19}$$

where

$$a(t) = \frac{1 + t/\pi - \sqrt{1 + 3t/\pi}}{2(1 - t/\pi)}. (20)$$

Note that a(t) is finite when $t = \pi$ (giving $a(\pi) = -1/8$), and $a \to -1/2$ as $t \to \infty$. This solution is symmetric about the imaginary axis since in the Pe $\to 0$ limit there is no advection of c. An example plot of the boundary shape in this limit is given the next Section.

6. Numerical solution for the evolving boundary

The numerical task is to approximate the map (15) by truncating the infinite series at n=N and determining the 2N+2 coefficients A(t), $a_0(t)$, ..., $a_N(t)$, $b_1(t)$, ..., $b_N(t)$ using (18) and the two constraint equations $A+a_0=1$ and the truncated version (i.e. summed up to n=N) of (17).

To obtain a further 2N equations from (18) the method of [23] is used: 2N points ζ_j , $j=1,\ldots,2N$, are distributed uniformly around the unit ζ -circle, so that (18) becomes a system of 2N coupled first-order ODEs in t. In practice the $\zeta_j=\exp(\theta_j)$ points are chosen such that $\theta_j\in [-\pi+\epsilon,\pi-\epsilon]$, where ϵ is small and positive in order to avoid the singularity in (15) when $\zeta=-1$ i.e. the point at infinity in the z-plane. Here, the MATLAB routine ode15i is used to solve this system of coupled ODEs with the choice $\epsilon=0.006$ and N=128.

Fig. 3 shows the evolution of the interface for the cases Pe = 0.25, 1 and 4 for the duration $0 \le t \le 5$. Also shown is the concentration field at t = 5 for each case and the streamlines of the flow. The streamlines are computed using the complex potential $F(\omega) = \omega$ together with the relations (11) and the numerical approximation of (15).

Fig. 4 compares the interface profiles for the three different values of Pe at t=5, and the Pe = 0 exact solution (19) and (20). Both Figs. 3 and 4 show the formation of 'scallop' shaped indentation in the dissolving wall with a steeper lip facing upstream and a shallower, more gradually varying lip downstream. The asymmetry becomes more pronounced as Pe increases owing to the advection of the c-field downstream by the uniform flow. For Pe = 4 there is very little dissolution upstream on x=0. The exact Pe = 0 exact solution profile closely resembles that of Pe = 0.25.

The rate at which surface area S is dissolved is

$$\frac{dS}{dt} = \operatorname{Pe} \int_{\partial S} |v_n| |dz|,$$

$$= \operatorname{Pe} \int_{-\pi}^{\pi} |v_n| d\theta,$$

$$= \int_{-\pi}^{\pi} \left| \frac{\partial c}{\partial r} \right|_{r=1} d\theta \equiv I(\operatorname{Pe}),$$
(21)

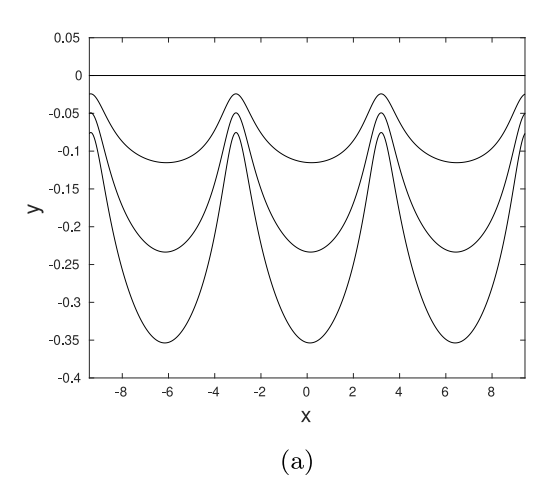
where (3) and (8) have been used, and I(Pe) is given by

$$I(Pe) = \frac{1}{2\pi} \int_{-\pi}^{\pi} \exp\left(\frac{Pe \sin \theta}{2 + 2\cos \theta}\right) K_1 \left[\frac{Pe}{\sqrt{2 + 2\cos \theta}}\right] \times \frac{Pe}{\sqrt{2 + 2\cos \theta}} d\theta$$

$$= \frac{Pe}{4\pi} \int_{-\pi}^{\pi} \exp\left(\frac{Pe}{2} \tan \frac{\theta}{2}\right) K_1 \left(\frac{Pe}{2} \sec \frac{\theta}{2}\right) \sec \frac{\theta}{2} d\theta. \quad (22)$$

In Appendix B it is shown that I(Pe)=1 for all Pe, and so (21) implies dS/dt=1, a general result which serves as a useful check on the numerical results. This result can alternatively be derived by integrating $v_n=-(\partial c/\partial n)$ around the boundary in the z-plane, and using the 2D divergence theorem to convert this boundary integral to the integral of $-\nabla^2 c$ over the area occupied by fluid. Then using (4) and treating the term involving $\partial c/\partial x$ by Green's theorem together with the condition c=0 on all boundaries, the result dS/dt=1 follows.

Fig. 5 shows the area lost to dissolution S(t) as a function of t computed by direct numerical evaluation of the interface area



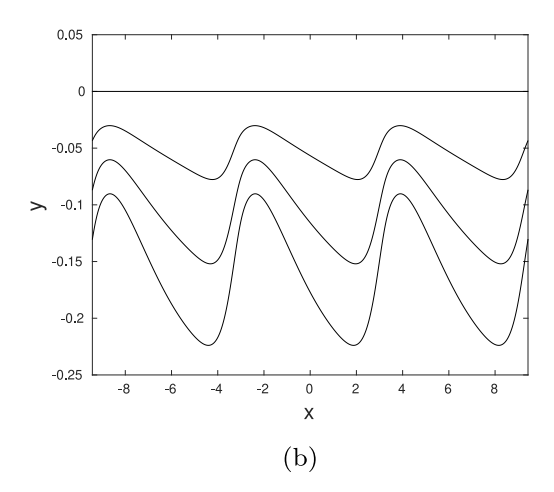


Fig. 6. Evolution of the interface pictured at equal time intervals up to t = 1, for periodically arranged sources at $z = 2n\pi + i$ in a uniform stream towards the positive real direction far from the wall. (a) Pe = 0.25 and (b) Pe = 4.

below the real axis. Also shown is the exact area loss S=t. The agreement is good for all values of Pe shown, demonstrating the accuracy of the numerical method.

7. Periodic forcing

The Green's function forcing found in the previous Secs. can be used to find the response of more general distributions of forcing. In this Section forcing is considered in the form of infinite periodic street of point sources located initially unit distance from the wall and distance 2π apart i.e. at $z=2n\pi+\mathrm{i}$, $n=-\infty,\ldots,\infty$. In the ω -plane the solution for c can be written in terms of an infinite sum based on (10), while the flow field has the same complex potential as a single source:

$$c = \frac{1}{2\pi} \sum_{n=-\infty}^{\infty} e^{[\operatorname{Re}(\omega) + 2n\pi]\operatorname{Pe}/2} \left(K_0 \left[\frac{\operatorname{Pe}}{2} |\omega + 2n\pi - i| \right] - K_0 \left[\frac{\operatorname{Pe}}{2} |\omega + 2n\pi + i| \right] \right),$$

$$F(\omega) = \omega. \tag{23}$$

Now introduce the conformal map (e.g. [24])

$$\omega = f(\zeta) = -i \log \left(\frac{\zeta - e^{-1}}{e^{-1}(\zeta - e)} \right), \tag{24}$$

which maps the interior of the unit ζ -disk to the semi-strip $-\pi \leq \text{Re}(\omega) \leq \pi$, $\text{Im}(\omega) > 0$, and which is 2π -periodic in the $\text{Re}(\omega)$ direction, and has the property f(0) = i. Thus in the ζ -plane the solution for c is

$$c = \frac{1}{2\pi} \sum_{n=-\infty}^{\infty} e^{\left[\operatorname{Re}(f(\zeta)) + 2n\pi\right] \operatorname{Pe}/2} \left(K_0 \left[\frac{\operatorname{Pe}}{2} |f(\zeta) + 2n\pi - i| \right] - K_0 \left[\frac{\operatorname{Pe}}{2} |f(\zeta) + 2n\pi + i| \right] \right). \tag{25}$$

Differentiation of (25) gives

$$\frac{\partial c}{\partial r}\Big|_{r=1} = -\frac{Pe}{2\pi} \sum_{n=-\infty}^{\infty} e^{[u+2n\pi]Pe/2} \times \frac{K_1 \left[\frac{Pe}{2} \sqrt{(u+2n\pi)^2 + 1}\right]}{\sqrt{(u+2n\pi)^2 + 1}} \left(\frac{e-e^{-1}}{e+e^{-1} - 2\cos\theta}\right), \tag{26}$$

where $u = u(\theta) = f(\exp(i\theta))$ is a real-valued function. The sum in (26) is straightforward to compute since the rapid decay

of the modified Bessel function for large argument implies that truncation of the infinite sum such that $n \in [-N, N]$, accurately approximates $\partial c/\partial r|_{r=1}$. Here N=50 is used.

As in the single source case, the form of the map from the unit ζ -disk to the physical z-plane is written in terms of an infinite series which is then approximated numerically. The following form is used

$$z = g(\zeta, t) = -i \log \left(\frac{\zeta - e^{a_0 - 1}}{e^{a_0 - 1} (\zeta - e^{1 - a_0})} \right) + i a_0 + i \sum_{n=1}^{\infty} (a_n + i b_n) \zeta^n,$$
(27)

with an initial flat interface giving conditions $a_n(0) = 0$ and $b_n(0) = 0$ for all n. Note that (27) has the required property g(0, t) = i.

As in the single source case, the map $g(\zeta,t)$ satisfies the Polubarinova–Galin equation

$$\operatorname{Re}\left[\overline{\zeta g'}\frac{\partial g}{\partial t}\right] = \sigma_p(\theta) \quad \text{on} \quad |\zeta| = 1, \tag{28}$$

where $\sigma_p(\theta) = -\partial c/\partial r|_{r=1}$ is given by (26).

The numerical solution of (28) proceeds as before with the infinite sum being truncated at n=M, giving 2M+1 unknowns $a_0, a_1, \ldots, a_M, b_1, \ldots, b_M$, and 2M+1 ODEs are formed by considering (28) at 2M+1 evenly spaced point around the unit ζ -circle. The ODE system is again solved using MATLAB's *ode15i* routine.

Examples of the surface evolution is given in Figs. 6(a) (Pe = 0.25) and 6(b) (Pe = 4). As expected, the asymmetry in the surface shape becomes more pronounced as Pe increases. It is interesting that, in contrast to a single source the scalloping is such that the steeper fluid–surface interface is downstream of the shallower interface. This is a consequence of the periodicity of the sources. For small times the surface shape takes the form of a small amplitude sine curve with troughs immediately below each source. For non-zero Pe the surface dissolves more quickly downstream of each source. This combined with periodicity implies that the interface must slope upwards more steeply than it does downwards.

8. Conclusions

The explicit solution for uniform steady flow past a point source of dissolving agent or heat, along with the conformally invariant governing equations is used to derive a Polubarinova-Galin equation for the time-dependent map which gives the

evolving shape of an initially straight surface. Typically a scallopshaped depression forms in the surface, with degree of asymmetry depending on Pe. More realistic representations of sources can be obtained by convolving the point source solution with a smooth and compact source distribution function. However, sufficiently far from the smooth source the resulting distribution of c will be similar to that of a point source and so the surface evolution will resemble that due to a point source.

An infinite street of point sources of c is shown to give rise to periodic scalloping patterns. While such an arrangement of seems unlikely in nature, it is interesting that such repeating scallop patterns are observed in nature. It is noted, however, that local shedding of vorticity (via viscous effects) is thought to be influential in the scalloping of soluble surfaces [25]. Moreover, as a precursor to scalloping, turbulent flow over a substrate which can either dissolve or melt has also shown to be unstable with viscosity determining the wavelength of instability [26].

The solutions presented here are the first to consider the case when c is concentrated at a point, and undergoes diffusion and advection by a background flow. A possible scenario where this may occur is on the surface of frozen lakes where the upwelling of warm water at a confined location in the lake's surface provides a localised source a warm water capable of melting surrounding 'slush' e.g. [3]. Spectacular ice-star patterns may arise from this process. However in such cases the dynamics appears to be more appropriately modelled by a point source for the fluid flow rather than a uniform flow at infinity as done here. This leads to another class of problems which could be considered using similar methods: when the fluid source is concentrated at a source and transports fluid with, say, c=1 at the source towards a surface where c=0. This is left for future work.

Declaration of competing interest

The authors declare that they have no known competing financial interests or personal relationships that could have appeared to influence the work reported in this paper.

Acknowledgements

NRMcD thanks the Isaac Newton Institute for Mathematical Sciences, Cambridge, UK, for support and hospitality during the 2019 programme 'Complex analysis: techniques, applications and computations' where discussion related to this work was had with fellow participants. The programme was supported by EP-SRC, UK grant no. EP/R014604/1. The authors thank the referees for their helpful comments.

Appendix A. Exact solution for Pe = 0

In the Pe \rightarrow 0 limit, the Polubarinova–Galin equation to be solved is, from (14),

$$\operatorname{Re}\left[\overline{\zeta f'(\zeta)}\frac{\partial f}{\partial t}\right] = \frac{1}{2\pi}, \quad \zeta = e^{\mathrm{i}\theta}. \tag{A.1}$$

With a constant on the RHS, (A.1) is equivalent to the Hele-Shaw free boundary flow (e.g. [18,19]) for a source of unit strength located a unit distance from an initially flat interface. An exact solution for a similar scenario obtained using the Schwarz function method appears in [27]. For convenience, and to accommodate changes in notation and that here the source is located above the interface, the details are reproduced in this appendix.

Let

$$z = f(\zeta, t) = iR\left(\frac{1}{1+\zeta} + a\zeta + d\right),\tag{A.2}$$

where R(t), a(t) and c(t) be real time-varying coefficients to be found. This truncated form of (15) turns out to be an exact solution in this case. Requiring that f(0, t) = i gives $R = (1+d)^{-1}$.

The Schwarz function of the curve representing the fluid-solid interface is the locally analytic function g(z,t) such that $g(z,t)=\bar{z}$ on the curve, and is obtained by taking the conjugate of (A.2), and using the fact that $\bar{\zeta}=\zeta^{-1}$ on the unit circle:

$$\bar{z} = g = -iR\left(\frac{\zeta}{1+\zeta} + \frac{a}{\zeta} + d\right)$$

$$= z - iRa(\zeta + \zeta^{-1}) - 2iRd - iR. \tag{A.3}$$

Demanding that the interface be aligned along the real axis as $z \to \infty$ requires that $g \to z$ as $\zeta \to -1$ and so d = a - 1/2 and R = 2/(1+2a). That the initial interface is flat gives a(0) = 0. The one-parameter form of the map is now determined as (19) and it remains to find a(t) where a(0) = 0.

In terms of the Schwarz function, free boundary Hele-Shaw flow satisfies (e.g. [18,19]) $\partial_t g = 2\partial_z w$, where $w = (1/2\pi)\log(z-i)$ is the complex potential in the limit $z \to i$ where the source is located. The singular behaviour on both sides of $\partial_t g = 2\partial_z w$ must match as $z \to i$. From (A.2) in the limit $z \to i$ or $\zeta \to 0$, $iR(a-1)(z-i)^{-1} \sim \zeta^{-1}$, and $\partial_t g = 2\partial_z w$ gives

$$\frac{d}{dt}\left(R^2a(a-1)\right) = \frac{1}{\pi}.\tag{A.4}$$

Integrating (A.4) and using R = 2/(1 + 2a) and a(0) = 0 gives a quadratic for a(t) with solution given by (20).

Appendix B. Derivation of $I(Pe) \equiv 1$

Let $\alpha = \text{Pe}/2$ so that the integral (22) becomes

$$I(\alpha) = \frac{\alpha}{2\pi} \int_{-\pi}^{\pi} \exp\left(\alpha \tan \frac{\theta}{2}\right) K_1\left(\alpha \sec \frac{\theta}{2}\right) \sec \frac{\theta}{2} d\theta.$$
 (B.1)

Differentiating (B.1) with respect to α and using $K'_1(z) = -K_0(z) - K_1(z)/z$ gives upon simplification

$$\begin{split} \frac{dI}{d\alpha} &= \frac{\alpha}{2\pi} \int_{-\pi}^{\pi} \exp\left(\alpha \tan \frac{\theta}{2}\right) \times \\ &\left[K_1 \left(\alpha \tan \frac{\theta}{2}\right) \tan \frac{\theta}{2} \sec \frac{\theta}{2} - K_0 \left(\alpha \tan \frac{\theta}{2}\right) \sec^2 \frac{\theta}{2} \right] d\theta. \end{split} \tag{B.2}$$

Using $dK_0(z)/dz = -K_1(z)$ observe that

$$\frac{\alpha}{2\pi} \int_{-\pi}^{\pi} \exp\left(\alpha \tan \frac{\theta}{2}\right) K_1\left(\alpha \tan \frac{\theta}{2}\right) \tan \frac{\theta}{2} \sec \frac{\theta}{2} d\theta = \\
-\frac{1}{\pi} \int_{-\pi}^{\pi} \exp\left(\alpha \tan \frac{\theta}{2}\right) \frac{d}{d\theta} K_0\left(\alpha \tan \frac{\theta}{2}\right) d\theta \tag{B.3}$$

Integrating the RHS of (B.3) by parts gives

$$\frac{\alpha}{2\pi} \int_{-\pi}^{\pi} \exp\left(\alpha \tan \frac{\theta}{2}\right) K_1\left(\alpha \tan \frac{\theta}{2}\right) \tan \frac{\theta}{2} \sec \frac{\theta}{2} d\theta = \frac{\alpha}{2\pi} \int_{-\pi}^{\pi} \exp\left(\alpha \tan \frac{\theta}{2}\right) K_0\left(\alpha \tan \frac{\theta}{2}\right) \sec^2 \frac{\theta}{2} d\theta, \tag{B.4}$$

where the property $K_0(z) \sim \sqrt{\pi/2z} \exp(-z)$ as $z \to +\infty$ has been used to show that the terms arising in integration by parts evaluated at $\theta = \pm \pi$ vanish. Hence (B.2) and (B.4) combine to give $I'(\alpha) = 0$.

Now, using $K_1(z) \sim 1/z$ as $z \to 0$ in (B.1) gives

$$\lim_{\alpha \to 0} I(\alpha) = \frac{\alpha}{2\pi} \int_{-\pi}^{\pi} \frac{1}{\alpha \sec \frac{\theta}{2}} \sec \frac{\theta}{2} d\theta = 1.$$
 (B.5)

Since $I'(\alpha) = 0$ and I(0) = 1, it follows $I(\alpha) = 1$ for all α i.e. for all Pe.

References

- [1] L. Ristroph, Sculpting with flow, J. Fluid Mech. 838 (2018) 1–4, http://dx.doi.org/10.1017/jfm.2017.890.
- [2] O. Devauchelle, A.P. Petroff, H.F. Seybold, D.H. Rothman, Ramification of stream networks, Proc. Natl. Acad. Sci. 109 (51) (2012) 20832–20836, http://dx.doi.org/10.1073/pnas.1215218109.
- [3] P. Grodzki, P. Szymczak, Reactive-infiltration instability in radial geometry: From dissolution fingers to star patterns, Phys. Rev. E 100 (2019) 033108, http://dx.doi.org/10.1103/PhysRevE.100.033108.
- [4] J.M. Huang, N.J. Moore, Morphological attractors in natural convective dissolution, Phys. Rev. Lett. 128 (2022) 024501, http://dx.doi.org/10.1103/ PhysRevLett.128.024501.
- [5] J.E. Laity, N.T. Bridges, Ventifacts on earth and mars: Analytical, field, and laboratory studies supporting sand abrasion and windward feature development, Geomorphology 105 (2009) 202–217, http://dx.doi.org/10.1016/j.geomorph.2008.09.014.
- [6] N. Goldenfeld, P.Y. Chan, J. Veysey, Dynamics of precipitation pattern formation at geothermal hot springs, Phys. Rev. Lett. 96 (2006) 254501, http://dx.doi.org/10.1103/PhysRevLett.96.254501.
- [7] P. Meakin, B. Jamtveit, Geological pattern formation by growth and dissolution in aqueous systems, Proc. R. Soc. A Math. Phys. Eng. Sci. 466 (2115) (2010) 659–694, http://dx.doi.org/10.1098/rspa.2009.0189.
- [8] R.L. Curl, Scallops and flutes, Trans. Cave Res. Group Great Br. 7 (1966) 121–160.
- [9] M. Bushuk, D.M. Holland, T.P. Stanton, A. Stern, C. Gray, Ice scallops: a laboratory investigation of the ice-water interface, J. Fluid Mech. 873 (2019) 942-976, http://dx.doi.org/10.1017/jfm.2019.398.
- [10] T.A. Douglas, M.T. Mellon, Sublimation of terrestrial permafrost and the implications for ice-loss processes on mars, Nature Commun. 10 (1) (2019) 1716. http://dx.doi.org/10.1038/s41467-019-09410-8.
- [11] L. Ristroph, M.N.J. Moore, S. Childress, M.J. Shelley, J. Zhang, Sculpting of an erodible body by flowing water, Proc. Natl. Acad. Sci. 109 (48) (2012) 19606–19609, http://dx.doi.org/10.1073/pnas.1212286109.
- [12] J.M. Huang, M.N.J. Moore, L. Ristroph, Shape dynamics and scaling laws for a body dissolving in fluid flow, J. Fluid Mech. 765 (2015) R3, http://dx.doi.org/10.1017/jfm.2014.718.
- [13] M.Z. Bazant, Conformal mapping of some non-harmonic functions in transport theory, Proc. R. Soc. Lond. Ser. A Math. Phys. Eng. Sci. 460 (2004) 1433–1452, http://dx.doi.org/10.1098/rspa.2003.1218.

- [14] J. Choi, D. Margetis, T.M. Squires, M.Z. Bazant, Steady advection-diffusion around finite absorbers in two-dimensional potential flows, J. Fluid Mech. 536 (2005) 155–184, http://dx.doi.org/10.1017/S0022112005005008.
- [15] L.M. Cummings, Y.E. Hohlov, S.D. Howison, K. Kornev, Two-dimensional solidification and melting in potential flows, J. Fluid Mech. 378 (1999) 1–18, http://dx.doi.org/10.1017/S0022112098003188.
- [16] C.H. Rycroft, M.Z. Bazant, Asymmetric collapse by dissolution or melting in a uniform flow, Proc. R. Soc. Lond. Ser. A Math. Phys. Eng. Sci. 472 (2016) 20150531, http://dx.doi.org/10.1098/rspa.2015.0531.
- [17] A.J.C. Ladd, L. Yu, P. Szymczak, Dissolution of a cylindrical disk in Hele-Shaw flow: a conformal-mapping approach, J. Fluid Mech. 903 (2020) A46, http://dx.doi.org/10.1017/jfm.2020.609.
- [18] S.D. Howison, Fingering in Hele-Shaw cells, J. Fluid Mech. 167 (1986) 439–453, http://dx.doi.org/10.1017/S0022112086002902.
- [19] B. Gustafsson, A. Vasiliev, Conformal and Potential Analysis in Hele-Shaw Cells, Birkhauser, Basel, 2009.
- [20] M.C. Dallaston, S.W. McCue, A curve shortening flow rule for closed embedded plane curves with a prescribed rate of change in enclosed area, Proc. R. Soc. Lond. Ser. A Math. Phys. Eng. Sci. 472 (2016) 20150629, http://dx.doi.org/10.1098/rspa.2015.0629.
- [21] M.Z. Bazant, J. Choi, B. Davidovitch, Dynamics of conformal maps for a class of non-Laplacian growth phenomena, Phys. Rev. Lett. 91 (2003) 045503, http://dx.doi.org/10.1103/PhysRevLett.91.045503.
- [22] S.J. Harris, N.R. McDonald, Fingering instability in wildfire fronts, J. Fluid Mech. 943 (2022) A34, http://dx.doi.org/10.1017/jfm.2022.452.
- [23] M.C. Dallaston, S.W. McCue, An accurate numerical scheme for the contraction of a bubble in a Hele-Shaw cell, in: Proceedings of the 16th Biennial Computational Techniques and Applications Conference, CTAC-2012, in: ANZIAM J., vol. 54, 2013, pp. C309-C326, http://dx.doi.org/10.21914/anziami.v54i0.6241.
- [24] P.J. Baddoo, L.J. Ayton, A calculus for flows in periodic domains, Theor. Comput. Fluid Dyn. 35 (2) (2021) 145–168, http://dx.doi.org/10.1007/ s00162-020-00551-x.
- [25] R.M. Thomas, Size of scallops and ripples formed by flowing water, Nature 277 (5694) (1979) 281–283, http://dx.doi.org/10.1038/277281a0.
- [26] P. Claudin, O. Durán, B. Andreotti, Dissolution instability and roughening transition, J. Fluid Mech. 832 (2017) R2, http://dx.doi.org/10.1017/jfm.2017.
- [27] N.R. McDonald, Computation of Hele-Shaw free boundary problems near obstacles, Theor. Comput. Fluid Dyn. 24 (6) (2010) 537–550, http://dx.doi. org/10.1007/s00162-010-0185-7.